

## Supporting Information

for

Directing self-assembly in solution towards improved cooperativity in Fe(III) complexes with  
amphiphilic tridentate ligands

Ana I. Vicente,<sup>a,b</sup> Xinwey Wu,<sup>a</sup> Yannick Ortin,<sup>c</sup> Liliana P. Ferreira,<sup>b,d</sup> Maria de Deus Carvalho,<sup>a</sup> Sara Realista,<sup>a,b</sup> Andrew Barker,<sup>c</sup> Grace G. Morgan,<sup>c</sup> Nuno Galamba,<sup>a,b</sup> Paulo J. Costa,<sup>a,b</sup> Maria José Calhorda<sup>a,b</sup>  
and Paulo N. Martinho<sup>\*a,b,c</sup>

- a. Centro de Química e Bioquímica, Faculdade de Ciências, Universidade de Lisboa, Campo Grande, 1749-016 Lisboa, Portugal.*
- b. Biosystems and Integrative Sciences Institute (BioISI), Faculdade de Ciências, Universidade de Lisboa, Campo Grande, 1749-016 Lisboa, Portugal.*
- c. School of Chemistry, University College Dublin, Belfield, D4, Dublin, Ireland.*
- d. Physics Department, University of Coimbra, 3004-516 Coimbra, Portugal.*
- e. Department of Inorganic Chemistry, Faculty of Science, Charles University, 128 43 Prague 2, Czech Republic.*

### Table of contents

1. Cyclic voltammetry studies	2
2. Variable UV-vis spectroscopy	3
3. Mössbauer spectroscopy	5
4. Particle size determination	7
5. Chronoamperometric studies	8
6. Scanning Electron Microscopy imaging	9
7. Molecular Dynamics	11

## 1. Cyclic voltammetry studies

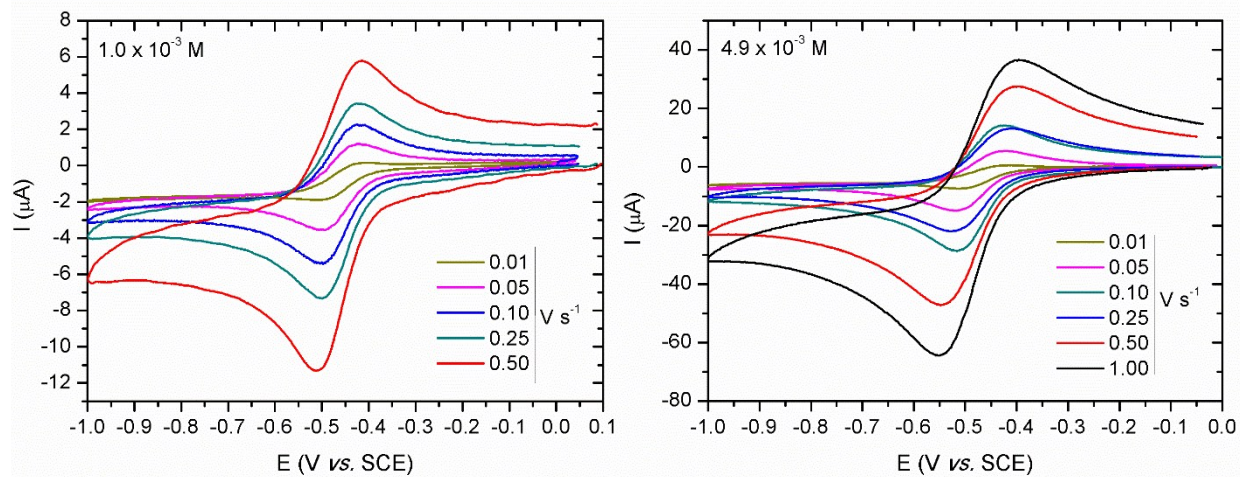


**Fig. S1** Cyclic voltammograms of **1** in dichloromethane at different scan rates using two different concentrations  $1 \times 10^{-3}$  M (left) and  $4.9 \times 10^{-3}$  M (right). Pt was used as working electrode (2 mm diameter), Pt wire and SCE as counter and reference electrodes, respectively.  $\text{NBu}_4\text{PF}_6$  was used as supporting electrolyte.

## 2. Variable temperature UV-vis spectroscopy

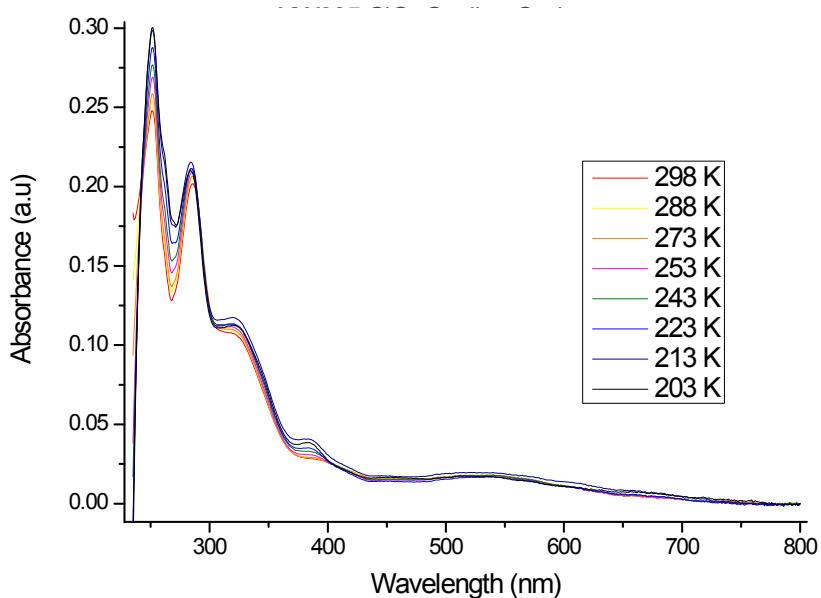


**Fig. S2** Variable temperature UV-vis spectra of **1** in a  $4.4 \times 10^{-6}$  M  $\text{CH}_2\text{Cl}_2$  solution (cooling mode).

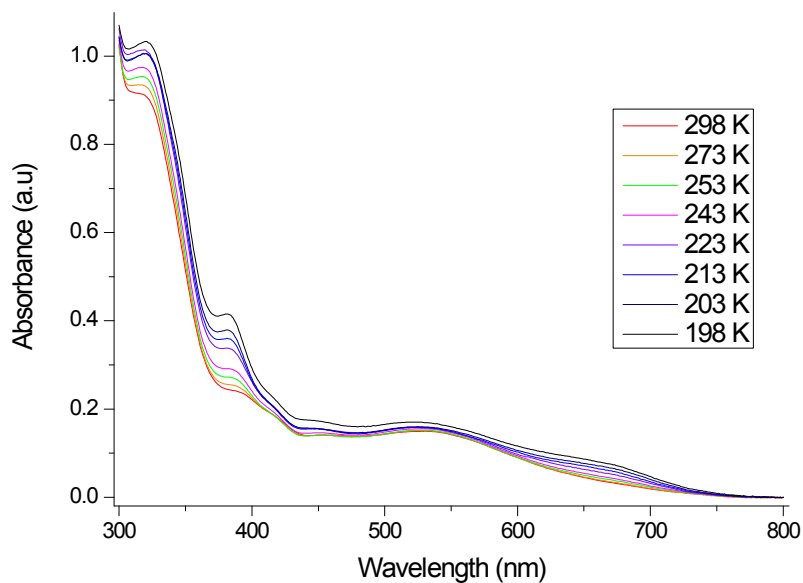


**Fig. S3** Variable temperature UV-vis spectra of **1** in a  $4.4 \times 10^{-5}$  M  $\text{CH}_2\text{Cl}_2$  solution (heating mode).

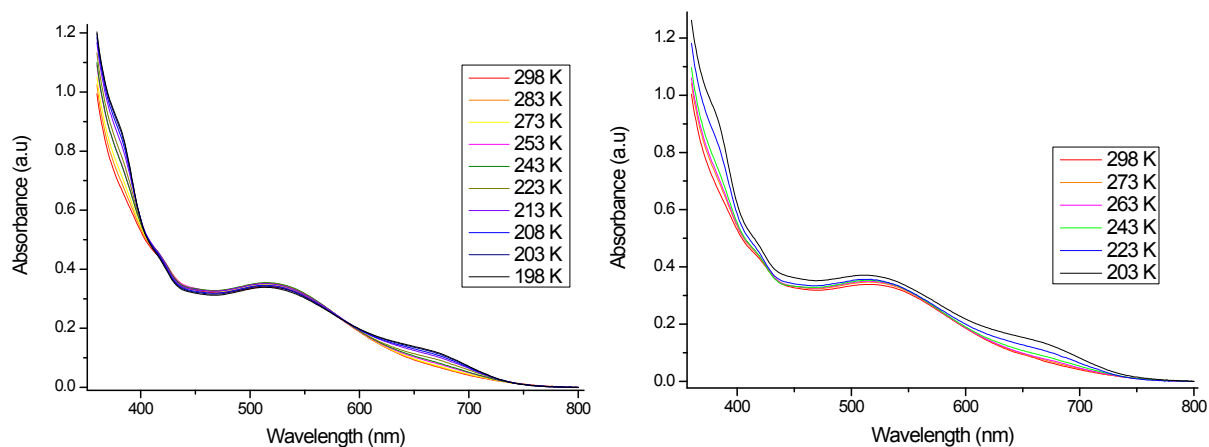


**Fig. S4** Variable temperature UV-vis spectra of **1** in a  $2.2 \times 10^{-4}$  M  $\text{CH}_2\text{Cl}_2$  solution. Left: cooling mode; Right: heating mode.

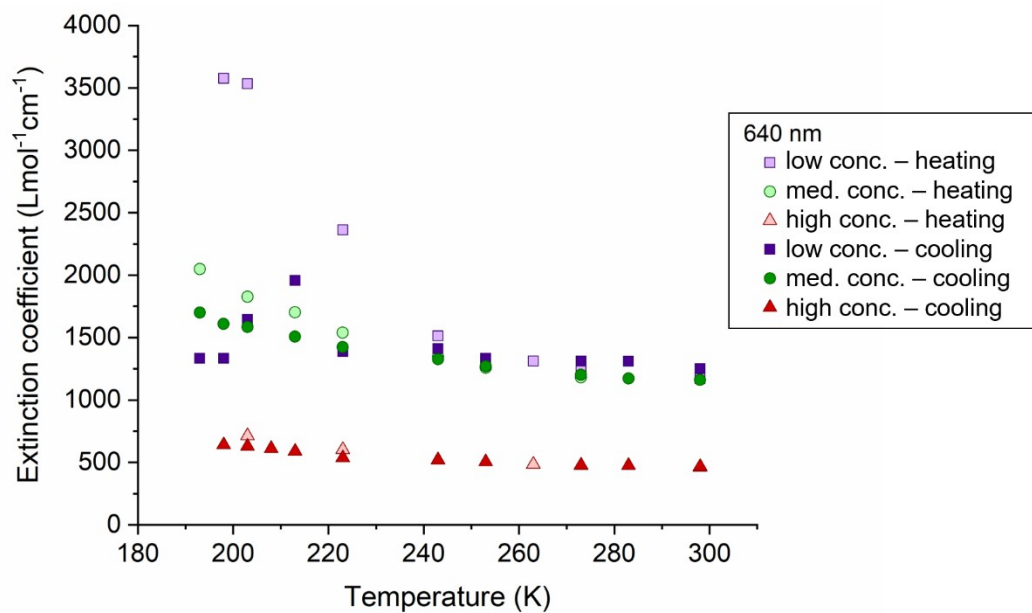


**Fig. S5** Extinction coefficient vs.  $T$  for **1** at low concentration ( $4.4 \times 10^{-6}$  M), medium concentration ( $4.4 \times 10^{-5}$  M) and high concentration ( $2.2 \times 10^{-4}$  M)  $\text{CH}_2\text{Cl}_2$  solutions both in the cooling and heating modes.

### 3. Mössbauer spectroscopy

The magnetic properties of **1** in the solid-state and as a frozen solution in  $\text{CH}_2\text{Cl}_2$  were investigated by Mössbauer spectroscopy. The  $^{57}\text{Fe}$  Mössbauer spectra were recorded at 78 K, in transmission mode, using a conventional constant-acceleration spectrometer and a 50 mCi  $^{57}\text{Co}$  source in a Rh matrix. The measurements were performed using a liquid nitrogen flow cryostat with a temperature stability of  $\pm 0.5$  K. The velocity scale was calibrated using an  $\alpha\text{-Fe}$  foil. The spectra were fitted to Lorentzian lines using the WinNormos software program, and the isomer shifts reported are relative to metallic  $\alpha\text{-Fe}$  at room temperature.

The Mössbauer spectra of both samples are shown in Fig. S6. For the solid sample (bottom figure) the spectrum is well fitted using two quadrupole doublets. The blue one, corresponding to around 60% of the iron nuclei, is characterized by an isomer shift ( $\delta$ ) value of  $0.22(1) \text{ mm s}^{-1}$  and a quadrupole splitting ( $\Delta E_Q$ ) of  $2.91(1) \text{ mm s}^{-1}$ , parameters characteristic of low-spin (LS) Fe ions. The remaining 40% of the iron nuclei, represented by the green sub-spectrum, has hyperfine parameters characteristic of Fe in the high-spin (HS) state ( $\delta = 0.42(4) \text{ mm s}^{-1}$  and  $\Delta E_Q = 0.45(4) \text{ mm s}^{-1}$ ). The frozen solution spectrum (top figure) is well fitted by a single quadrupole doublet displaying hyperfine parameters ( $\delta = 0.21(2) \text{ mm s}^{-1}$ ;  $\Delta E_Q = 2.81(4) \text{ mm s}^{-1}$ ) very close to the ones characterizing the LS state of the Fe ions of the solid sample, although with a much larger Lorentzian line width (Table S1). This much larger quadrupole doublet, when compared to the one of the solid compound, is interpreted not only as the result of being a measure of a frozen liquid but also as an indication of an existing fraction of a HS iron component, although in lower percentage than in the solid sample. The line broadening asymmetry has been previously found in other LS Fe(III) compounds,<sup>1-4</sup> and this asymmetry was attributed to the relatively long paramagnetic relaxation times of the iron when compared to the  $^{57}\text{Fe}$  nuclear Larmor precession time.

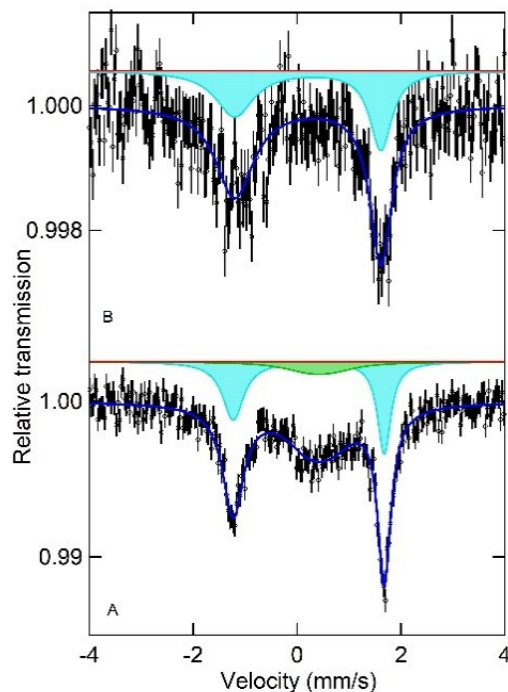


**Fig. S6**  $^{57}\text{Fe}$  Mössbauer spectra collected at 78 K of A) solid sample of **1** and B) frozen solution (glass) of **1** in  $\text{CH}_2\text{Cl}_2$ .

**Table S1** Hyperfine parameters extracted from fitting the Mössbauer spectra shown in Fig. S6:  $\delta$  - isomer shift;  $\Delta E_Q$  - quadrupole splitting;  $\Gamma$  - Lorentzian line width at half maximum;  $W_{21}$ : width of line 2 relative to line 1;  $I$  - relative intensity (uncertainty < 2%). Statistical errors are given in parentheses.

Sample	Fe subspectrum	$\delta$ (mm/s)	$\Delta E_Q$ (mm/s)	$\Gamma$ (mm/s)	$W_{12}$ (mm/s)	$I$ (%)
Solid	blue	0.22(1)	2.91(1)	0.49(3)	0.63(4)	58.8
	green	0.42(4)	0.45(4)	1.2(4)	-	41.2
Frozen solution in $\text{CH}_2\text{Cl}_2$	blue	0.21(2)	2.81(4)	0.89(9)	0.58(6)	100

#### 4. Particle size determination

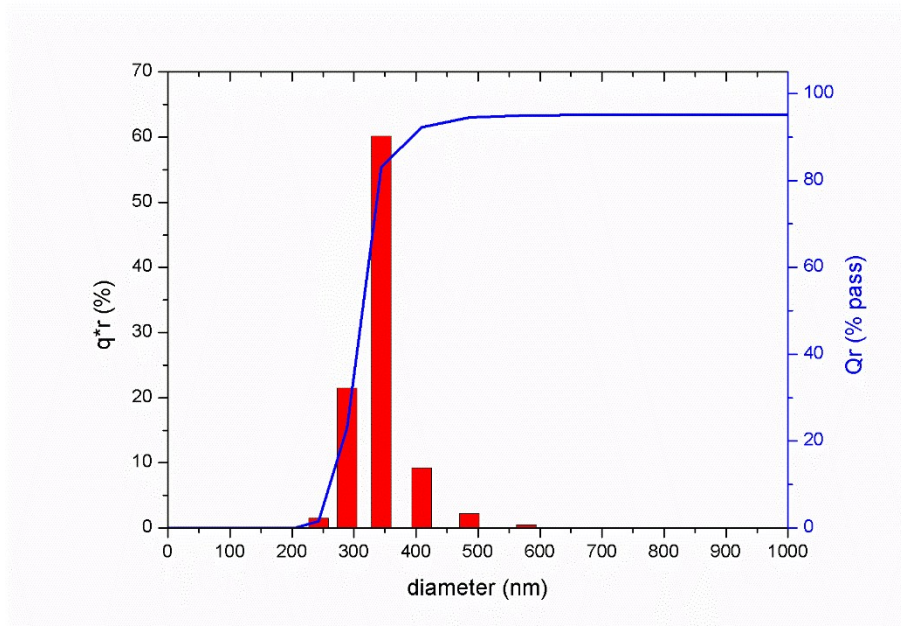


**Fig. S7** Size distribution of particles of **1** in a  $4.9 \times 10^{-3}$  M  $\text{CD}_2\text{Cl}_2$  solution.

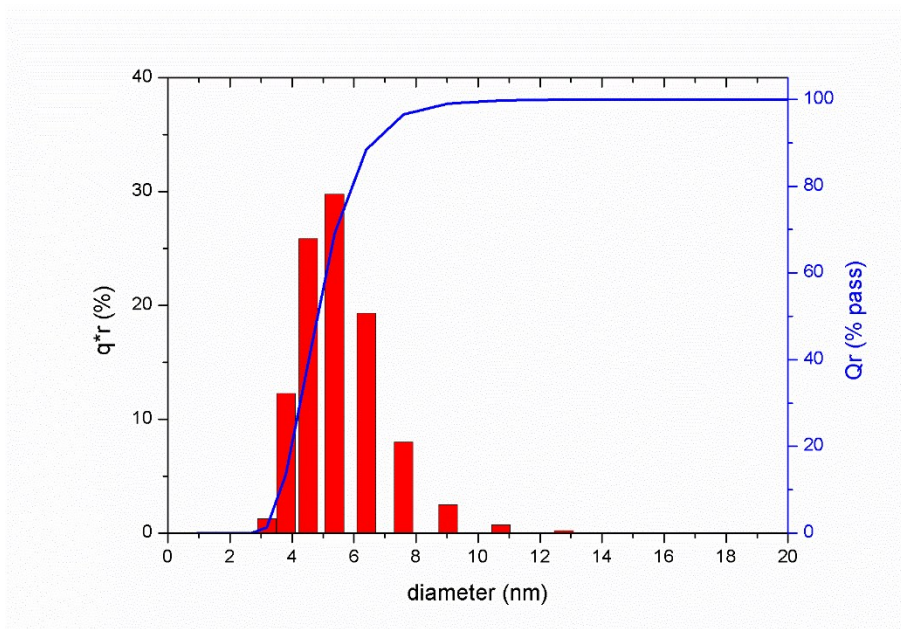


**Fig. S8** Size distribution of particles of **1** in a  $4.4 \times 10^{-5}$  M  $\text{CH}_2\text{Cl}_2$  solution.

## 5. Chronoamperometric studies

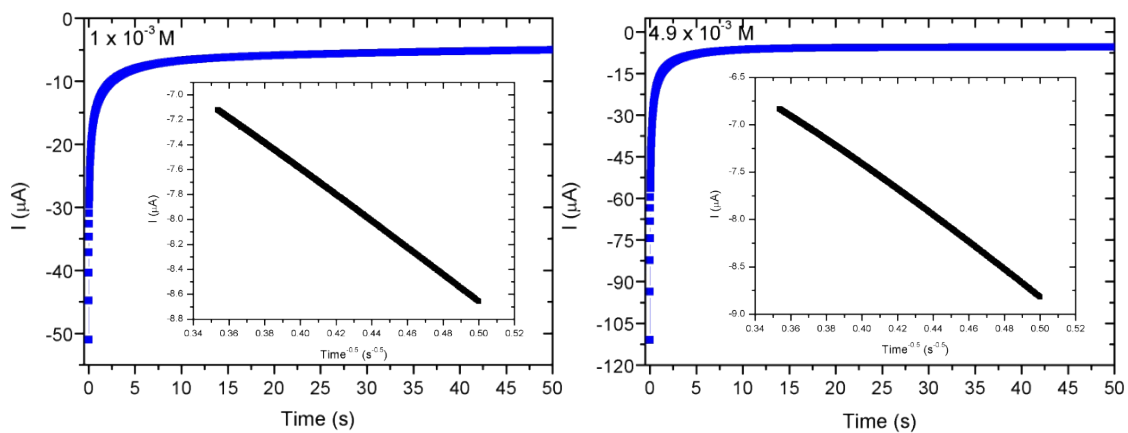


**Fig. S9** Chronoamperograms of **1** in dichloromethane using two different concentrations  $1 \times 10^{-3} \text{ M}$  (left) and  $4.9 \times 10^{-3} \text{ M}$  (right). Inset: plot of current,  $I$ , versus  $t^{0.5}$ , data collected between 4 and 8 s. Pt was used as working electrode (2 mm diameter), Pt wire and SCE as counter and reference electrodes, respectively.  $\text{NBu}_4\text{PF}_6$  was used as supporting electrolyte.

## 6. Scanning Electron Microscopy imaging

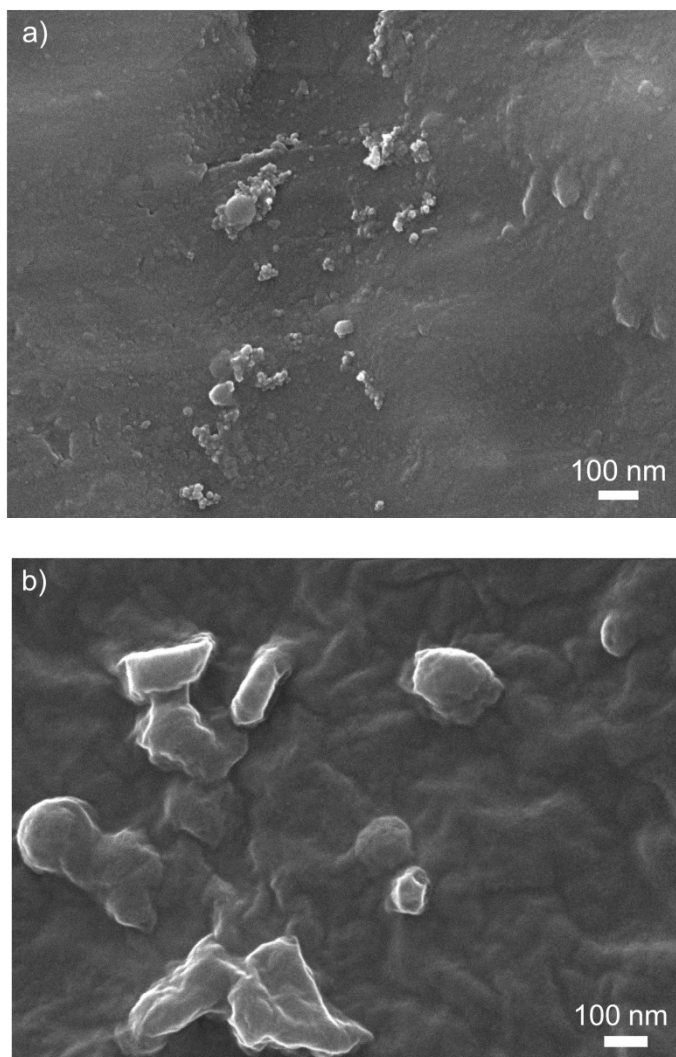


**Fig. S10** SEM images of aggregates of a  $4.4 \times 10^{-5}$  M  $CD_2Cl_2$  of **1**; a) magnification 30000x and b) magnification 30000x.

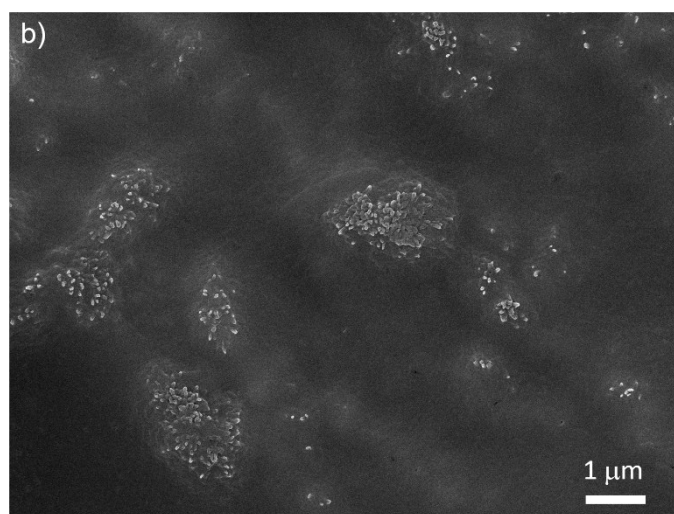
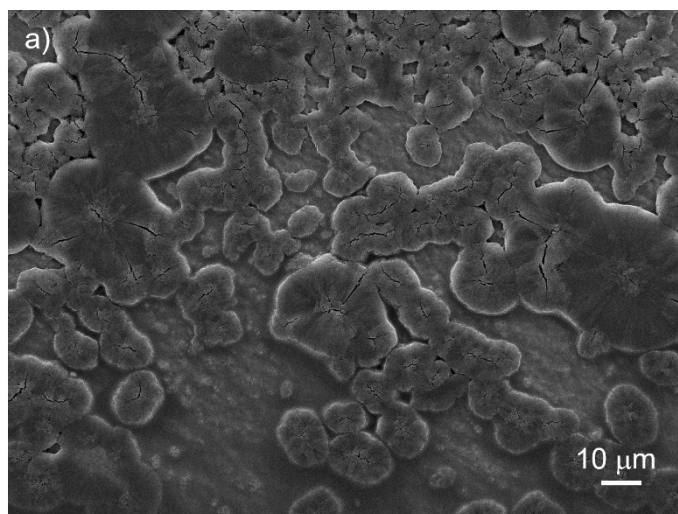


**Fig. S11** SEM images of aggregates of a  $4.9 \times 10^{-3}$  M  $\text{CD}_2\text{Cl}_2$  solution of **1**: a) magnification 500x and b) magnification 5000x.

## 7. Molecular Dynamics

The capped head and tail groups used to calculate the atomic charges are shown in Fig. S12. The force field was derived for the high spin state of the amphiphilic complex. Thus, the geometry of the capped head group used to calculate the charges was optimized for the high spin state. This geometry depicts a bond elongation of  $\sim 10\%$  for the 2 Fe-N<sub>imine</sub> bonds and a  $\sim 12\%$  and  $\sim 15\%$  elongation for the Fe-N<sub>amine</sub> bonds, whereas an elongation of  $\sim 2.5\%$  is observed for the Fe-O bonds, relative to the low spin state.

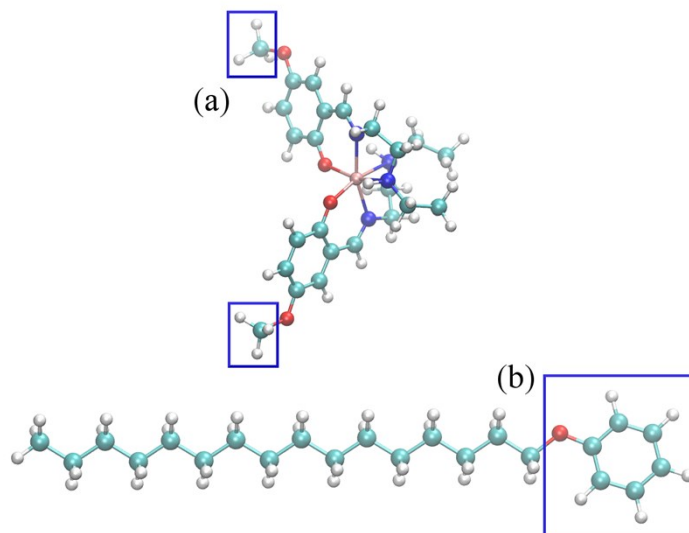


**Fig. S12** (a) Fe(III) complex head capped with a CH<sub>3</sub> group and (b) tail capped with a C<sub>6</sub>H<sub>6</sub>-O group, used to calculate the atomic charges. The atomic charges of the head were obtained through the RESP method by constraining the Fe atomic charge to + 2.0e and those of the tail were obtained with AM1-BCC.

The electrostatic potential (ESP) charge of Fe was found to be +1.4 e and the RESP charge was < +0.1 e. A radius of 1.5 Å, 2.0 Å, and 2.5 Å, were used for Fe, for comparison purposes, showing no significant influence on the Merz-Kollman charge. Furthermore, similar results are found when the charges are calculated for the complex and for the capped head. Thus, because of the low value of the RESP charge on the Fe atom, and the fact that ESP charges are difficult to assess for buried atoms the charge on the Fe atom was constrained to the value of +2.0e in the RESP approach. This value, while somewhat arbitrary, was observed from Mulliken population analysis, reflecting a milder charge transfer, relative to the ESP charge. The charge of -1e of the complex was achieved, upon combination of the RESP (head) and AM1-BCC (tail) charges, by absorbing the excess negative charge ( $\sim -0.05e$ ) to the Fe atom leading to a final charge on the Fe atom of +1.95e.

The opbe/cc-pvtz optimized Fe-X covalent bonds (X = N, O) length and the (Fe-X-Y) and (X-Fe-X) angles (Y=C, H) were adopted. The respective force constants were defined to be 700.0 kcal.mol<sup>-1</sup>.Å<sup>-2</sup> and 90.0 kcal.mol<sup>-1</sup>.rad<sup>-2</sup>. These values were defined based on preliminary simulations insuring geometrical stability of the octahedral metal centre. The bond and angle force constants were systematically increased until no significant geometry distortions, ending with LINCS instability and ultimately bond breaking, were observed. The dihedral angles and force constants involving the Fe atom were set to zero as these were found to be unimportant for the geometrical stability of the head group. Although the above bond and angle force constants could in principle be derived more rigorously from electronic structure calculations, their improvement should have no influence on the self-assembling of the complex, which is the main

purpose of the MD simulations reported here.

The force field for the perchlorate anions and dichloromethane were also derived based on the GAFF protocol.

#### References

1. M. Griffin, S. Shakespeare, H. J. Shepherd, C. J. Harding, J. F. Létard, C. Desplanches, A. E. Goeta, J. a K. Howard, A. K. Powell, V. Mereacre, Y. Garcia, A. D. Naik, H. Müller-Bunz and G. G. Morgan, *Angew. Chem. Int. Ed.*, 2011, 50, 896–900
2. Y. Maeda, N. Tsutsumi and Y. Takashima, *Inorg. Chem.*, 1984, 23, 2440–2447.
3. M. D. Timken, D. N. Hendrickson and E. Sinn, *Inorg. Chem.*, 1985, 24, 3947–3955.
4. M. D. Timken, A. M. Abdel-Mawgoud and D. N. Hendrickson, *Inorg. Chem.*, 1986, 25, 160–164.